Article

Analysis of the Internal Structure of Hadrons Using Direct Photon Production

David Francisco Rentería-Estrada [1,†] , **Roger José Hernández-Pinto** [1,*,†] and **German Sborlini** [2,3,†]

1   Facultad de Ciencias Físico-Matemáticas, Universidad Autónoma de Sinaloa, Ciudad Universitaria,
    CP 80000 Culiacán, Mexico; davidrenteria.fcfm@uas.edu.mx
2   Instituto de Física Corpuscular, Universitat de València—Consejo Superior de Investigaciones Científicas,
    Parc Científic, E-46980 Paterna, Spain; german.sborlini@desy.de
3   Deutsches Elektronen-Synchrotron, DESY, Platanenallee 6, D-15738 Zeuthen, Germany
*   Correspondence: roger@uas.edu.mx
†   These authors contributed equally to this work.

Abstract: Achieving a precise description of the internal structure of hadrons is crucial for deciphering the hidden properties and symmetries of fundamental particles. It is a hard task since there are several bottlenecks in obtaining theoretical predictions starting from first principles. In order to complement highly accurate experiments, it is necessary to use ingenious strategies to impose constraints from the theory side. In this article, we describe how photons can be used to unveil the internal structure of hadrons. We explore how to describe NLO QCD plus LO QED corrections to hadron plus photon production at colliders and discuss the impact of these effects on the experimental measurements.

Keywords: hadron production; photon production; QCD corrections; NLO calculations

1. Introduction and Motivation

Understanding the internal structure of non-fundamental particles implies dealing with complex models, for which the solutions cannot be easily obtained, even if they take advantage of the fascinating simplifications introduced by gauge symmetries. Roughly speaking, starting from the accepted framework to describe all of the fundamental particles, namely the Standard Model (SM), it is not clear how to model strongly interacting systems from first principles. The typical energy scale associated withthese systems is in between the low and the high-energy regimes. For both, we can successfully evaluate the proper limits of SM and use approximated methods to solve the resulting equations, although a satisfactory description in the whole energy range is still missing.

A widely applied strategy to describe the internal structure of hadrons relies on the parton model, which is based on the study of the distribution of partons (i.e., fundamental particles such as quarks and gluon) inside the hadrons. These distributions are extracted from the experiments, by using advanced fitting and modelling methods [1] and by includ-ing spin information within the polarized parton distribution functions (PDF). However, this methodology is not enough to explain the total spin of the proton. Using up-to-date experimental data, it turns out that only about 30% of the proton total spin can be explained by the quarks. Moreover, as shown in References [2,3], data extracted from deep-ineslastic scattering (DIS) experiments is not enough to constrain the shape of polarized quark and gluon distributions. A precise description of such distributions is crucial to tackle the *proton spin crisis*, a long-standing problem in which the solution still eludes the efforts of the scientific community.

In order to shed light onto possible solutions to the spin crisis and to obtain more information about the internal dynamics of hadrons, we need to access parton level kine-matics in the most clean and unperturbed manner. It is a well-known fact that high-energy collisions of hadrons produce a hot and dense medium mainly composed of strongly

interacting particles. As a consequence, any particle that couples to QCD partons suffer from this interaction. The main problem is that such states cannot be easily described within the perturbative approach, thus introducing huge uncertainties in its theoretical modelling. Even if there were very recent and precise descriptions of Quark-Gluon Plasma (QGP) evolution using hydrodynamic and AdS/CFT-inspired models [4,5], their consistent combination with the customary perturbative approach is not well understood. For these reasons, one clever alternative to overcome these issues relies on the measurement of final states involving hard photons. These particles are almost transparent to the QGP states, thus allowing us to access parton-level kinematics in a cleaner manner.

This work is based on Reference [6] and constitutes a step towards a more complete and up-to-date description of the phenomenology of hadron–photon production at colliders. The use of photons as clean probes has been explored in several works to establish patterns of energy loss in heavy ion collisions [7], the sensitivity to medium-induced modifications to fragmentation functions (FF) [8–10], and the constraint of photon fragmentation in hadron colliders [11], among other studies. Here, we focus on the production of a direct photon plus one hadron including next-to-leading order (NLO) corrections due to QCD effects. This is an interesting observation since it involves both PDFs and FFs, which allows us to obtain constraints for such distributions. Thus, in Section 2, we explain the theoretical framework applied to calculate the NLO corrections to the cross section as well as the inclusion of sub-dominant QED corrections. Special emphasis is put on the isolation algorithm that allows us to efficiently separate the contribution due to direct photon emissions from the one originating from hadron decays. In Section 3, we present some numerical results using up-to-date PDFs and FFs, comparing them to the ones presented in Reference [6]. Finally, in Section 4, we summarize this presentation and explain future strategies to explore the inner structure of hadrons by using this observation.

2. Implementation of the Computation

Our computation is based on the parton model for describing hadron–hadron collisions in a high-energy regime. In such a kinematic regime, there are factorization properties [12] that allow us to apply perturbation theory to compute the cross section. The factorization theorems have been rigorously proven for DIS using the method of operator product expansions (OPE). However, neither the extension to hadron–hadron collisions nor the one including fragmentation into hadrons have been formally demonstrated. In any case, several studies [13,14] have explored potential factorization-breaking issues, and they have shown that these problems might appear beyond NLO when color-charged particles are involved.

Explicitly, the cross section is described by a convolution between PDFs, FFs, and the *partonic* cross section. All of the non-perturbative effects associated to the low-energy interaction inside the hadrons are included within the PDFs and FFs, whilst the partonic cross section can be computed using the perturbative framework. Thus, in the case of hadron–photon production, we can start writing

$$d\sigma^{\mathrm{DIR}}_{H_1 H_2 \to h\,\gamma} \quad = \quad \sum_{a_1 a_2 a_3} \int dx_1 dx_2 dz\, f^{(H_1)}_{a_1}(x_1, \mu_I) f^{(H_2)}_{a_2}(x_2, \mu_I)\, d^{(h)}_{a_3}(z, \mu_F) d\hat{\sigma}^{\mathrm{DIR}}_{a_1 a_2 \to a_3\,\gamma}\,, \tag{1}$$

with H_1 and H_2 as the hadrons colliding in the initial state, a_i as the partons involved in the process, and $d\hat{\sigma}^{\mathrm{DIR}}$ as the differential partonic cross section. The function $f^{(H)}_a(x, \mu_I)$ represents the PDF associated to the collinear emission of a parton of flavor a from the hadron H with momentum fraction x at the initial factorization scale μ_I. Analogously, $d^{(h)}_a(z, \mu_F)$ represents the density probability function generating a hadron h with momentum fraction z from the parton a at the final factorization scale μ_F. Regarding the scale dependence, the partonic cross section includes terms depending on μ_I and μ_F and on the renormalization scale, μ_R.

This formula assumes that the photon is directly generated in the parton interaction but that additional contributions could arise. For instance, high-energy collisions of hadrons

could originate pions, which may eventually decay into photons. Thus, if we look for final state high-energy photons, our measurements could also include contributions from this decay process. Due to the quantum nature of the process that we explore, it is not possible to identify the true origin of the particles that we observe in the detector. Thus, in principle, we must also compute the fragmentation or *resolved* component of the cross section, i.e.,

$$
d\sigma^{\mathrm{RES}}_{H_1 H_2 \to h\,\gamma} \;=\; \sum_{a_1 a_2 a_3 a_4} \int dx_1 dx_2 dz dz'\, f^{(H_1)}_{a_1}(x_1, \mu_I) f^{(H_2)}_{a_2}(x_2, \mu_I)
$$
$$
\times d^{(h)}_{a_3}(z, \mu_F) d^{(\gamma)}_{a_4}(z', \mu_F) d\hat{\sigma}_{a_1 a_2 \to a_3 a_4}\,,
\tag{2}
$$

where the parton a_4 generates a photon after hadronization. Notice the presence of the parton-to-photon fragmentation function, $d^{(\gamma)}_a(z, \mu_F)$. This quantity is not very well constrained experimentally due to non-perturbative and low-energy effects. Additionally, strictly speaking, we should include a component originating from a non-perturbative hadronization process leading to the desired final state, i.e., a purely non-perturbative generation of one hadron plus an energetic photon. In any case, beyond the leading order, the separation in direct, resolved, or double-resolved components is not physical. However, it is possible to efficiently suppress the resolved contribution, relying on so-called isolation prescriptions.

2.1. Isolation and Direct Photon Contribution

When QCD partons interact, they usually generate highly energetic states that very quickly recombine to produce new hadrons. If the detector is hit by a photon, we could use this fact to discriminate its origin. When the photon is generated as a consequence of a QCD-mediated decay, several particles are produced close to the photon. On the other hand, if the photon was generated in a pure partonic process, then it is expected to leave a clean signal in the detector. It is possible to show that there is a high correlation among direct photon production and *isolated* photons. By definition, isolated photons are those that fulfill certain selection criteria, establishing a separation from this particle to any hadron or jet. Usually, distances are measured within the rapidity–azimuthal plane: if $a = (\eta_1, \phi_1)$ and $b = (\eta_2, \phi_2)$, then

$$
\Delta r_{ab} = \sqrt{(\eta_1 - \eta_2)^2 + (\phi_1 - \phi_2)^2}\,,
\tag{3}
$$

represents the distance between these two points. Different definitions of distance are available, but this one is especially suitable for experiments where angular variables can be efficiently measured.

There are several criteria in the market, such as the cone isolation or the smooth isolation prescription. The latest, introduced for the first time in Reference [15], posses several theoretical advantages. The selection procedure goes as follow:

1. Identify each photonic signal in the final state, and draw a cone of radius r_0 around it.
2. If there are not QCD partons inside the cone, the photon is isolated.
3. If there are QCD partons inside the cone, we calculate their distance to the photon, r_j, following Equation (3) and then we define the total transverse hadronic energy for a cone of radius r as

$$
E_T(r) = \sum_j E_{T_j} \theta(r - r_j)\,,
\tag{4}
$$

   where E_{T_j} is the transverse energy of the jth QCD parton inside the cone.
4. Define an arbitrary smooth function $\xi(r)$ that satisfies $\xi(r) \to 0$ for $r \to 0$.
5. If $E_T(r) < \xi(r)$ for every $r < r_0$ (i.e., for any point inside the fixed cone), then the photon is isolated.

This algorithm is known as *smooth* cone isolation because it forces the QCD partons to have less transverse energy as they are emitted closer to the photons. The fixed cone

introduces a static cutoff, and this might lead to problems from the theory side. The smooth cone isolation allows for soft gluons in any region of the phase space, leading to an IR-safe definition of the cross section, especially when higher-order corrections are considered. Additionally, this prescription completely eliminates the collinear quark radiation, which implies that the fragmentation contribution in Equation (2) can be neglected. In this way,

$$d\sigma_{H_1 H_2 \to h \gamma} = \sum_{a_1 a_2 a_3} \int dx_1 dx_2 dz \, f_{a_1}^{(H_1)}(x_1, \mu_I) f_{a_2}^{(H_2)}(x_2, \mu_I) \, d_{a_3}^{(h)}(z, \mu_F) d\hat{\sigma}_{a_1 a_2 \to a_3 \gamma}^{\mathrm{ISO}},\tag{5}$$

represents the full contribution to the cross section when only isolated prompt photons are measured, completely removing the resolved component and simplifying the calculation.

Finally, we would like to comment on the choice of the isolation prescription. Even if the smooth cone isolation seems to be perfectly suitable for theoretical calculations, it has several limitations from the experimental side. Specifically, a high angular resolution is required to implement the condition of Equation (4). Thus, most of the experimental collaborations still rely on fixed cone strategies. However, several studies were performed to compare both approaches, finding that the differences can be minimized or directly neglected for some observables [16,17].

2.2. Higher-Order Corrections

Once the observable has been properly defined, we can discuss how to introduce higher-order corrections to Equation (5). Let us consider the Born level kinematic given by

$$H_1(K_1) + H_2(K_2) \to h(K_3) + \gamma(K_4),\tag{6}$$

with K_i as the four momenta of the different particles in the lab frame. When we apply the parton model, we introduce the momentum fractions x_1 and x_2 for the incoming partons and z for the final-state parton that hadronizes into h. Thus, we can write

$$a_1(x_1 K_1) + a_2(x_2 K_2) \to a_3(K_3/z) + \gamma(K_4),\tag{7}$$

for the parton kinematics. As usual, the calculation is performed in the partonic center-of-mass frame and then boosted to the lab frame. In this work, we first focus our attention to the QCD corrections to the process $\gamma + h$, up to NLO accuracy. Thus, the partonic cross section can be expanded according to

$$
\begin{aligned}
d\hat{\sigma}_{a_1 a_2 \to a_3 \gamma}^{\mathrm{ISO}} = {} & \frac{\alpha_S}{2\pi} \frac{\alpha}{2\pi} \int dPS^{2 \to 2} \frac{|\mathcal{M}^{(0)}|^2(x_1 K_1, x_2 K_2, K_3/z, K_4)}{2\hat{s}} \mathcal{S}_2 \\
& + \frac{\alpha_S^2}{4\pi^2} \frac{\alpha}{2\pi} \int dPS^{2 \to 2} \frac{|\mathcal{M}^{(1)}|^2(x_1 K_1, x_2 K_2, K_3/z, K_4)}{2\hat{s}} \mathcal{S}_2 \\
& + \frac{\alpha_S^2}{4\pi^2} \frac{\alpha}{2\pi} \sum_{a_5} \int dPS^{2 \to 3} \frac{|\mathcal{M}^{(0)}|^2(x_1 K_1, x_2 K_2, K_3/z, K_4, k_5)}{2\hat{s}} \mathcal{S}_3,
\end{aligned}\tag{8}
$$

with $\hat{s}$ as the partonic center-of-mass energy, $|\mathcal{M}^{(0)}|^2$ as the squared matrix-element at the Born level, and $|\mathcal{M}^{(1)}|^2$ as the corresponding one-loop one. $\mathcal{S}_2$ and $\mathcal{S}_3$ are the measure functions that implement the experimental cuts and the isolation prescription for the $2 \to 2$ and $2 \to 3$ sub-processes, respectively. There are two partonic channels contributing at LO,

$$q\bar{q} \to \gamma g, \quad qg \to \gamma q,\tag{9}$$

whilst

$$q\bar{q} \to \gamma g g, \quad qg \to \gamma g q, \quad gg \to \gamma q\bar{q}, \quad q\bar{q} \to \gamma Q\bar{Q}, \quad qQ \to \gamma q Q,\tag{10}$$

are all of the QCD channels contributing at NLO. The opening of new channels could result in enhanced effects due to gluon PDFs.

In order to implement the NLO QCD corrections, we relied on the FKS subtraction algorithm [18], which splits the real emission phase space into different regions containing non-overlapping singularities and cancels them with local IR counter-terms. The renormalization was performed within the $\overline{\text{MS}}$ scheme.

On top of that, we also explored the impact of QED corrections. Going back to Equation (8), we appreciate that the NLO QCD contributions and LO QED corrections might have a similar weight due to the relation $\alpha_S^2 \alpha \approx \alpha^2 \approx \mathcal{O}(10^{-4})$. Of course, photon PDF is suppressed w.r.t. the QCD ones because of the sub-leading role of the electromagnetic interactions in the determination of the inner structure of hadrons. In any case, it constitutes a nonnegligible correction due to the high accuracy in experiments nowadays. Thus, we add to Equation (8)

$$d\hat{\sigma}_{a_1 a_2 \to a_3 \gamma}^{\text{ISO,QED}} = \frac{\alpha^2}{4\pi^2} \int dPS^{2\to 2} \frac{|\mathcal{M}_{QED}^{(0)}|^2(x_1 K_1, x_2 K_2, K_3/z, K_4)}{2\hat{s}} \mathcal{S}_2,$$

associated to the new partonic channel

$$q\gamma \to \gamma q, \quad q\bar{q} \to \gamma\gamma. \tag{11}$$

Regarding the second channel, we neglect its contribution by looking into charged hadrons in the final state. This is because such a sub-process involves the fragmentation of a photon into a hadron, which is also suppressed by the fact that electromagnetic interactions are sub-leading in the hadronization process. Furthermore, we assume that electromagnetic contribution to the hadronization is almost negligible compared to photon production from hadrons. We defer to future works for a deeper study of this assertion.

3. Numerical Simulations

The computation described in Section 2 was implemented in a Monte Carlo integrator, based on the one developed in Reference [6]. For the isolation algorithm, we used the function

$$\xi(r) = \epsilon_\gamma E_T^\gamma \left(\frac{1 - \cos(r)}{1 - \cos r_0} \right)^4, \tag{12}$$

with the parameters $\epsilon_\gamma = 1$, $r_0 = 0.4$, and the photon transverse energy E_T^γ. The average of the photon and hadron transverse energy was used as the typical energy scale of the process,

$$\mu \equiv \frac{p_T^h + p_T^\gamma}{2}, \tag{13}$$

and we set by default $\mu_I = \mu_F = \mu_R \equiv \mu$. It is worth appreciating that different isolation algorithms lead to similar results, given the fact that we restrict our attention to the computation of infrared-safe observations. This is because the resolved contribution given by Equation (2) tends to be highly suppressed by isolation procedures. On the other hand, our primary objective is obtaining access to the colliding-parton kinematics: the presence of an additional convolution with the parton-to-photon fragmentation functions leads to a more cumbersome relation between the original momentum fractions x_1 and x_2 and the external, measurable observations. For this reason, we keep the isolation algorithm fixed and focus on the effects due to the presence of NLO QCD and LO QED corrections. Explicit details about the comparison of different isolation algorithms for infrared-safe observations can be found in Reference [16].

Due to the fact that the production probability of heavy hadrons is very suppressed, we focus on the the process $p + p \to \pi + \gamma$, including the possibility of charge selection for the pion. Regarding the cuts, our default configuration corresponds to the ones used by the PHENIX detector:

- Pion and photon rapidities are restricted to $|\eta| \leq 0.35$.
- The photon transverse momentum fulfills $5\,\text{GeV} \leq p_T^\gamma \leq 15\,\text{GeV}$.

- Pion transverse momentum must be larger than 2 GeV.
- We consider full azimuthal coverage, i.e., no restriction on $\{\phi^\pi, \phi^\gamma\}$, as a simplification of the real detectors.

The lower cut on the pion transverse momentum is set to reduce the contamination from the non-perturbative processes. A similar argument holds for the limitation in the photon energy range. Regarding the center-of-mass energy of the hadron collisions, we use by default $E_{CM} = 200$ GeV, although we also explored the TeV region accessible by LHC, setting $E_{CM} = 13$ TeV.

As already proposed in Reference [6], we restrict $\Delta\phi$ in order to keep those events where the photon and the pion are produced in an almost back-to-back configuration: $\Delta\phi = |\phi^\pi - \phi^\gamma| \geq 2$. This is because the LO kinematics in the partonic center-of-mass frame allows for only back-to-back events; thus, imposing that restriction on $\Delta\phi$ is equivalent to looking around the Born kinematics.

Finally, we performed an update in the PDF and FF available in the original version of the code [6]. In particular, we switched from the standalone implementations of the different PDFs to the `LHAPDF` framework [19]. This allows us to unify the treatment of the PDFs and to simplify the numerical evaluations in the different scenarios. Moreover, we implemented in the code the updated set of FFs, `DSS2014` [20].

Phenomenology and Results

First, we reproduced the old results obtained with `MSTW2008NLO` PDFs [21] and `DSS2007` fragmentations [22] but using the new Monte Carlo implementation within the `LHAPDF` framework. Then, we explored the effects introduced by switching to novel versions of the PDFs and FFs. In particular, we considered three configurations:

1. σ_a: `NNPDF3.1` and `DSS2014` (default up-to-date simulation)
2. σ_b: `NNPDF3.1` and `DSS2007` (effects in the hadronization)
3. σ_c: `MSTW2008` and `DSS2014` (effects in the parton distributions)

We always used the corresponding sets with NLO QCD corrections. First, we considered the kinematics for the PHENIX experiment, focusing on pp collisions at $E_{CM} = 200$ GeV. In Figures 1 and 2, we plot the differential cross section as a function of p_T^π and p_T^γ, respectively. We restricted our attention to the NLO QCD corrections for the process $pp \to \gamma + \pi^+$ and used the default scale choice (as explained in the previous section).

Regarding the p_T^π spectrum for the three scenarios, we found that they are pretty similar. In fact, the absolute difference is smaller than 15% in the range $5\,\text{GeV} \leq p_T^\pi \leq 15\,\text{GeV}$. From the right plot in Figure 1, we notice that the `MSTW2008` PDF tends to slightly enhance the high-p_T region (i.e., $p_T^\pi \approx 13$ GeV) whilst the effect of the `DSS2007` FF goes in the opposite direction. Namely, `DSS2007` gives a larger cross section for low p_T and a smaller for high p_T, reaching a relative difference of $\mathcal{O}(10\%)$. In any case, it seems that the integrated effect seems to compensate across the whole range of p_T^π.

On the other hand, if we look at the p_T^γ spectrum, we find greater deviations from the default configuration. As shown in the right plot of Figure 2, the cross section is about 12% bigger when using the `DSS2007` fragmentations, and the trend ncreases with the photon transverse momentum. When we switch to `MSTW2008` PDFs, we also find that the cross section is higher than for the default configuration and that the trend increases with p_T^γ: the relative difference is $\mathcal{O}(7\%)$.

The comparison among the three PDF-FF scenarios show that there is room to impose tighter constraints on both the PDFs and FFs from PHENIX kinematic. However, given the fact that new colliders extend the available energy range, we studied the differences in the p_T^π spectrum at LHC, namely setting $E_{CM} = 13$ TeV whilst keeping the same angular resolution used for the PHENIX experiment. The results are shown in Figure 3, where we restricted the attention to σ_a and σ_c. Namely, we compared `NNPDF3.1` (blue line) and `MSTW2008` (orange line), keeping the same fragmentation functions. The differences are around 10%, with an enhancement of the cross section for $p_T^\pi \approx 13$ GeV for σ_a w.r.t. σ_c. As

already observed in Figures 1 and 2, it is worth noticing that we did not use DSS2007 for LHC energies because most of the events involve momentum fractions lying outside the validity range of the interpolator.
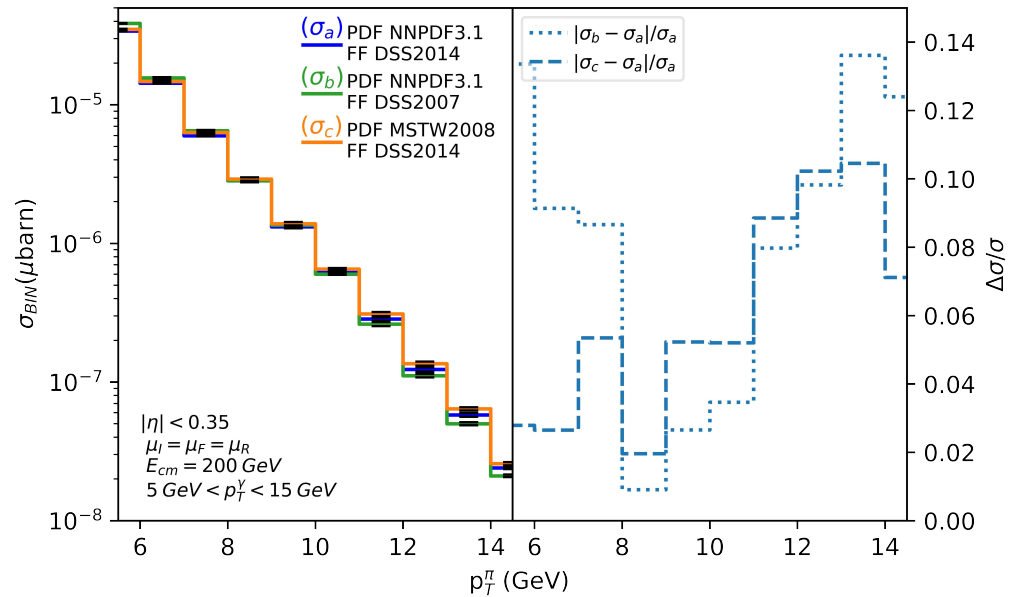
Figure 1. NLO QCD corrections to the p_T^{π} distribution of $pp \to \gamma + \pi^+$ for PHENIX kinematics ($E_{CM} = 200\,\text{GeV}$) in three different scenarios. In the right panel, we show the relative difference w.r.t. the default configuration (i.e., NNPDF3.1 PDF and DSS2014 FF).
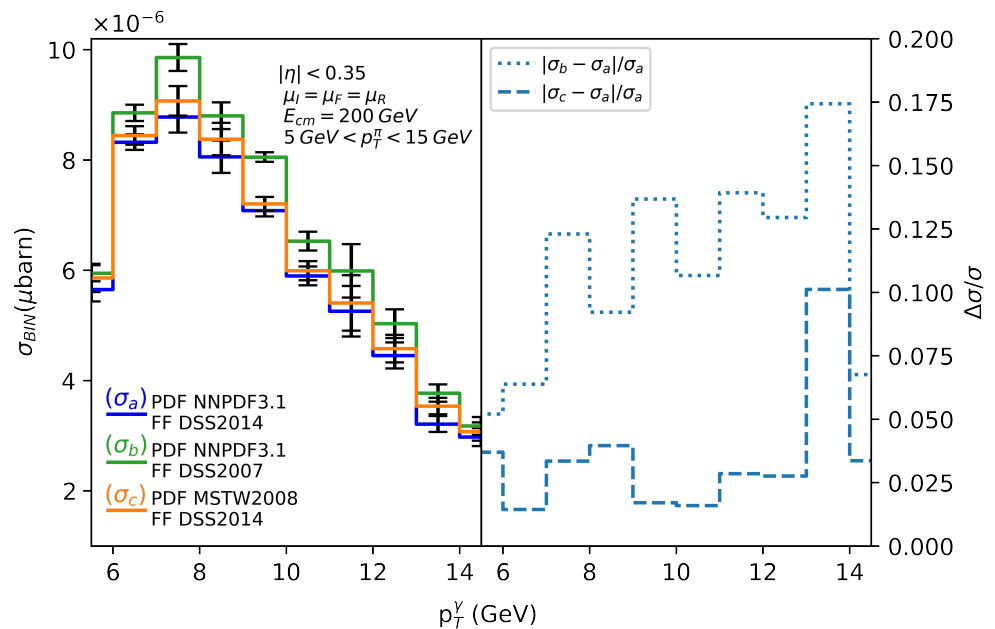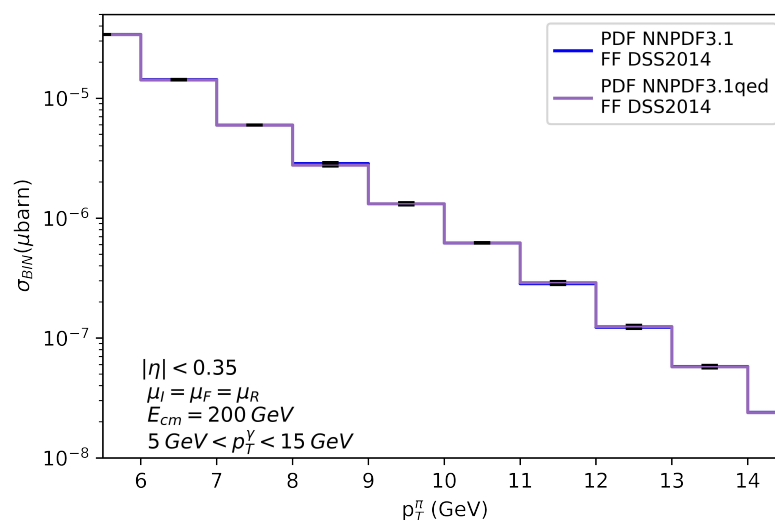

Figure 2. NLO QCD corrections to the p_T^{γ} distribution of $pp \to \gamma + \pi^+$ for PHENIX kinematics ($E_{CM} = 200\,\text{GeV}$) in three different scenarios. In the right panel, we show the relative difference w.r.t. the default configuration (i.e., NNPDF3.1 PDF and DSS2014 FF).
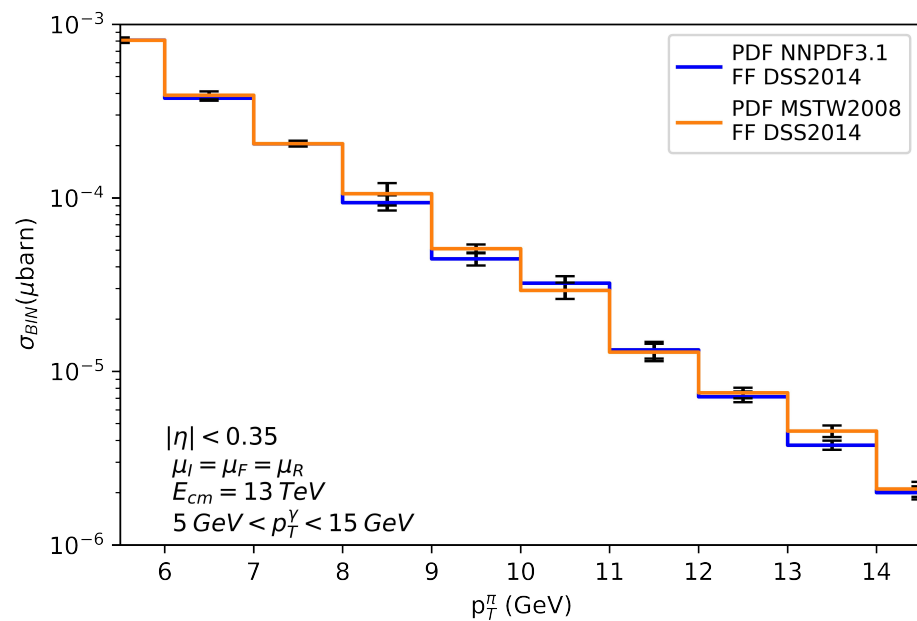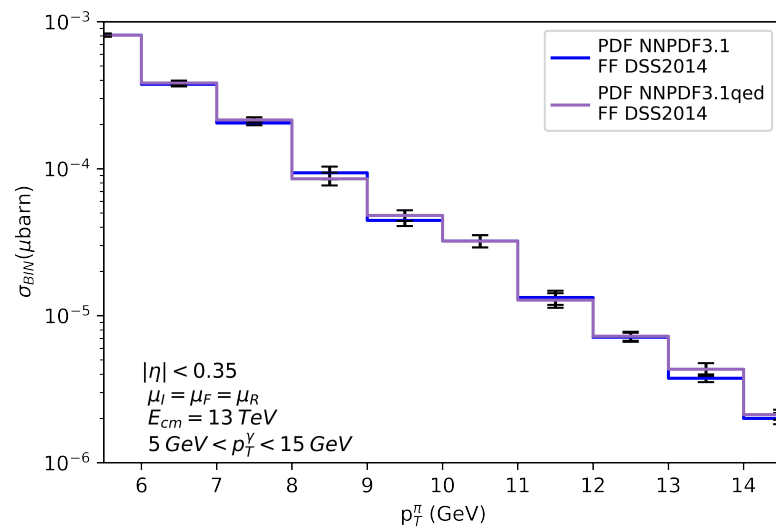
Figure 3. NLO QCD corrections to the p_T^π distribution of $pp \to \gamma + \pi^+$ for LHC kinematics ($E_{CM} = 13\,\text{TeV}$, angular constraints identical to those used for PHENIX) in three different scenarios. The relative differences are shown in the right panel.

Finally, we explored the impact of the combined NLO QCD + LO QED corrections on the process $pp \to \gamma + \pi^+$. In order to deal with the photon distribution, we switched to `NNPDF3.1luxQEDNLO` [23–25], which also include lepton densities. In our analysis, we leave aside lepton-initiated processes, since their contribution is very suppressed compared to the QCD one. The inclusion of such corrections is deferred for future studies. We compare the p_T^π spectrum at $E_{CM} = 200\,\text{GeV}$ (Figure 4) and $E_{CM} = 13\,\text{TeV}$ (Figure 5) for proton–proton collisions extrapolating the typical PHENIX cuts. We found corrections of $\mathcal{O}(2\%)$ for $E_{CM} = 200\,\text{GeV}$, whilst they increase to $\mathcal{O}(9\%)$ for LHC energies. This is partially due to the behavior of the QED and QCD couplings, which goes in opposite directions as the process energy increases. The weight of QED corrections tends to be slightly higher in the high-p_T region, although it seems to be more affected by the center-of-mass energy of the collision.

Figure 4. Comparison of the combined NLO QCD + LO QED (blue line) vs. the pure NLO QCD corrections to the p_T^π distribution of $pp \to \gamma + \pi^+$ in the PHENIX kinematics ($E_{CM} = 200\,\text{GeV}$). We use as a shorthand notation `NNPDF3.1qed` for `NNPDF3.1luxQEDNLO`.

Figure 5. Comparison of the combined NLO QCD + LO QED (blue line) vs. the pure NLO QCD corrections to the p_T^π distribution of $pp \to \gamma + \pi^+$ in the LHC kinematics ($E_{CM} = 13\,\text{TeV}$). We use as a shorthand notation `NNPDF3.1qed` for `NNPDF3.1luxQEDNLO`.

4. Conclusions and Outlook

In this article, we discussed the phenomenology of photon–hadron production in hadron colliders, centering on the process $pp \to \gamma + \pi^+$. We included NLO QCD and LO QED corrections to keep the effects of order $\alpha^2 \approx \alpha_S^2 \alpha$ under control. The results were compared with previous studies performed in Reference [6]. In both cases, we relied on the smooth isolation algorithm to get rid of the resolved component at NLO. The purpose of this strict restriction was to obtain access to the colliding-partons kinematics, which can be achieved more transparently by focusing on the direct production mechanism.

As a first step, we updated the Monte Carlo implementation to include the unified framework `LHAPDF` and the new set of pion FFs of `DSS2014`. We carefully studied the dependence of the PDF and FF sets by looking at the p_T^π and p_T^γ distributions. We found reasonable deviations (i.e., $\mathcal{O}(10\%)$ on average), although our preliminary studies suggest a stronger sensibility in the p_T^γ distribution.

Then, we included the LO QED corrections by opening the partonic channel $q\gamma$. We used the `NNPDF3.1luxQEDNLO` PDF set and tested the impact of these contributions on the p_T^π spectrum. We restricted our attention to the production of positive pions, since we claim that such a choice would heavily suppress any contribution associated to the hadronization process $\gamma \to \pi$. Comparing the corrections at pp colliders, we found small but still nonnegligible corrections: $\mathcal{O}(2\%)$ for PHENIX and $\mathcal{O}(8\%)$ for LHC center-of-mass energies.

The results presented in this article suggest that hadron+photon production might be a useful process to impose tighter constraints on both PDFs and FFs, something that could help enormously in unveiling the hidden properties and symmetries of hadrons. An extensive study for different observables could lead to an enhanced sensitivity on the PDFs through a careful reconstruction of the partonic momentum fractions. Further developments on these directions are being performed by our group.

Author Contributions: Implementation of the code, D.F.R.-E. and R.J.H.-P.; formulation of the problem, R.J.H.-P. and G.S.; writing, D.F.R.-E., R.J.H.-P. and G.S.; plots and figures, D.F.R.-E. All authors have read and agreed to the published version of the manuscript.

References

1. NNPDF Collaboration; Khalek, R.A.; Ball, R.D.; Carrazza, S.; Forte, S.; Giani, T.; Kassabov, Z.; Nocera, E.R.; Pearson, R.L.; Wilson, M.; et al. A first determination of parton distributions with theoretical uncertainties. *Eur. Phys. J. C* **2019**, *79*, 838. [CrossRef]
2. de Florian, D.; Sassot, R.; Stratmann, M.; Vogelsang, W. Global Analysis of Helicity Parton Densities and Their Uncertainties. *Phys. Rev. Lett.* **2008**, *101*, 072001. [CrossRef] [PubMed]
3. de Florian, D.; Sassot, R.; Stratmann, M.; Vogelsang, W. Extraction of Spin-Dependent Parton Densities and Their Uncertainties. *Phys. Rev. D* **2009**, *80*, 034030. [CrossRef]
4. Maldacena, J.M. The Large N limit of superconformal field theories and supergravity. *Adv. Theor. Math. Phys.* **1998**, *2*, 231–252. [CrossRef]
5. Bertoldi, G.; Bigazzi, F.; Cotrone, A.L.; Edelstein, J.D. Holography and unquenched quark-gluon plasmas. *Phys. Rev. D* **2007**, *76*, 065007. [CrossRef]
6. de Florian, D.; Sborlini, G.F.R. Hadron plus photon production in polarized hadronic collisions at next-to-leading order accuracy. *Phys. Rev. D* **2011**, *83*, 074022. [CrossRef]
7. Wang, X.-N.; Huang, Z.; Sarcevic, I. Jet quenching in the opposite direction of a tagged photon in high-energy heavy ion collisions. *Phys. Rev. Lett.* **1996**, *77*, 231–234. [CrossRef]
8. Arleo, F.; Aurenche, P.; Belghobsi, Z.; Guillet, J.-P. Photon tagged correlations in heavy ion collisions. *JHEP* **2004**, *11*, 009. [CrossRef]
9. Arleo, F. Hard pion and prompt photon at RHIC, from single to double inclusive production. *JHEP* **2006**, *9*, 15. [CrossRef]
10. Zhang, H.; Owens, J.F.; Wang, E.; Wang, X.-N. Tomography of high-energy nuclear collisions with photon-hadron correlations. *Phys. Rev. Lett.* **2009**, *103*, 032302. [CrossRef]
11. Belghobsi, Z.; Fontannaz, M.; Guillet, J.P.; Heinrich, G.; Pilon, E.; Werlen, M. Photon—Jet Correlations and Constraints on Fragmentation Functions. *Phys. Rev. D* **2009**, *79*, 114024. [CrossRef]
12. Collins, J.C.; Soper, D.E.; Sterman, G.F. Factorization of Hard Processes in QCD. *Adv. Ser. Direct. High Energy Phys.* **1989**, *5*, 1–91.
13. Catani, S.; de Florian, D.; Rodrigo, G. Space-like (versus time-like) collinear limits in QCD: Is factorization violated. *JHEP* **2012**, *7*, 26. [CrossRef]
14. Forshaw, J.R.; Seymour, M.H.; Siodmok, A. On the Breaking of Collinear Factorization in QCD. *JHEP* **2012**, *11*, 66. [CrossRef]
15. Frixione, S. Isolated photons in perturbative QCD. *Phys. Lett. B* **1998**, *429*, 369–374. [CrossRef]
16. Cieri, L. Diphoton isolation studies. *Nucl. Part. Phys. Proc.* **2016**, *273–275*, 2033–2039. [CrossRef]
17. Catani, S.; Cieri, L.; de Florian, D.; Ferrera, G.; Grazzini, M. Diphoton production at the LHC: A QCD study up to NNLO. *JHEP* **2018**, *4*, 142. [CrossRef]
18. Frixione, S.; Kunszt, Z.; Signer, A. Three jet cross-sections to next-to-leading order. *Nucl. Phys. B* **1996**, *467*, 399–442. [CrossRef]
19. Buckley, A.; Ferrando, J.; Lloyd, S.; Nordstrom, K.; Page, B.; Rufenacht, M.; Schonherr, M.; Watt, G. LHAPDF6: Parton density access in the LHC precision era. *Eur. Phys. J. C* **2015**, *75*, 132. [CrossRef]
20. de Florian, D.; Sassot, R.; Epele, M.; Hernández-Pinto, R.J.; Stratmann, M. Parton-to-Pion Fragmentation Reloaded. *Phys. Rev. D* **2015**, *91*, 014035. [CrossRef]
21. Martin, A.D.; Stirling, W.J.; Thorne, R.S.; Watt, G. Parton distributions for the LHC. *Eur. Phys. J. C* **2009**, *63*, 189–285. [CrossRef]
22. de Florian, D.; Sassot, R.; Stratmann, M. Global analysis of fragmentation functions for protons and charged hadrons. *Phys. Rev. D* **2007**, *76*, 074033. [CrossRef]
23. Manohar, A.V.; Nason, P.; Salam, G.P.; Zanderighi, G. The Photon Content of the Proton. *JHEP* **2017**, *12*, 46. [CrossRef]
24. NNPDF Collaboration; Bertone, V.; Carrazza, S.; Hartland, N.P.; Rojo, J. Illuminating the photon content of the proton within a global PDF analysis. *SciPost Phys.* **2018**, *5*, 8. [CrossRef]
25. Buonocore, L.; Nason, P.; Tramontano, F.; Zanderighi, G. Leptons in the proton. *JHEP* **2020**, *8*, 19. [CrossRef]